Controls by saturation state on etch pit formation during calcite dissolution

H. Henry Teng*

Department of Earth & Environmental Sciences, The George Washington University, Washington, DC 20006 USA

Abstract—Dissolution experiments were conducted on $\{10\bar{1}4\}$ cleavage faces of calcite at various under-saturations to determine how the saturation state controls etch pit formation. Experimental observations were made by using in situ fluid cell Atomic Force Microscopy. Three dissolution modes were observed. When the saturation index $\Omega > 0.541$, no etch pit formation was seen and dissolution primarily occurred at existing steps. When Ω decreased to $\Omega_c = 0.541-0.410$, the first visible pits appeared and continuous reduction in saturation state slowly increased the pit density on terraces while dissolution simultaneously proceeded at step edges. Finally, when the saturation state fell below $\Omega_{max} = \sim0.007$, a precipitous increase in pit density took place that sharply contrasted to the ordered fashion of pit formation observed at saturation conditions above this level. These observations are interpreted to be two-dimensional and unassisted pit formation at $\Omega < \sim0.007$, defect- and step-assisted dissolution in between $\Omega = 0.541$ and 0.007, and existing step-induced dissolution for $\Omega > 0.541$.

The values of Ω_c are in good agreement with the dislocation theory's predicted critical under-saturations for pit formation at line dislocations. The occurrence of Ω_{max} is not directly predicted but is a logical consequence of dissolution thermodynamics. These findings suggest that (1) dissolution near and far from equilibrium (i.e., $\Omega > \Omega_c$, $\Omega < \Omega_{max}$) is not controlled by dislocations, therefore (2) dislocation density should significantly impact dissolution rate only in the saturation range of $\Omega_{max} < \Omega < \Omega_c$; (3) dissolution kinetics and chemical affinity of dissolution reactions should have a non-linear relationship: at sufficiently close to equilibrium, when dislocations cannot open up to form etch pits, the dissolution kinetics will be limited by the number of existing steps; at far from equilibrium, when pits are able to form in defect-free regions, the dissolution rate will be capped by the maximum number of achievable steps.

These findings may provide explanations for several well-observed geochemical relationships, including the weak dependence of dissolution rate upon dislocation density in distilled water and the 'plateau' behavior of dissolution kinetics both near and far from equilibrium. The explosive occurrence of unassisted pit nucleation at $\Omega \sim \Omega_{max}$ is not predicted by the current dissolution rate equations. This suggests that an accurate 'general' rate law describing universal dissolution processes has yet to be developed. *Copyright © 2004 Elsevier Ltd*

1. INTRODUCTION

Chemical weathering affects global cycling of elements, compositions and nutrition availability of natural waters, soil formation, and atmospheric CO_2 concentrations (Garrels and Mackenzie, 1971; Berner et al., 1983; Lasaga et al., 1994). As such, considerable attention has been paid to mineral dissolution in the past quarter century. Extensive studies investigating various aspects of the dissolution processes have been carried out and a recurring theme among these investigations concerns understanding the mineral surface behavior during dissolution. To date, major findings show that dissolution preferentially occurs at specific surface sites that are characterized as having 'excess surface energy' (Holdren and Berner, 1979). This suggests that dissolution is directly controlled by surface reactions at these active sites. These sites include defects, dislocations, and grain boundaries (Helgeson et al., 1984) and are revealed by etch pits of various types developed on dissolved mineral surfaces (e.g., Berner, 1981; Brantley et al., 1986; Gratz et al., 1990, 1991; Hillner et al., 1992; Stipp et al., 1994; Lee and Parsons, 1995; Teng et al., 1997; Nugent et al., 1998). The nearly ubiquitous occurrence of etching features on both laboratory dissolved and naturally weathered mineral grains has led

researchers to believe that surface reaction-controlled processes are responsible for the dissolution of various minerals (e.g., Holdren and Berner, 1979; Lasaga et al., 1994; Brady and House, 1995; Brantley and Chen, 1995; Nugent et al., 1998).

One issue that has previously been neglected to a rather large extent is the controls of saturation state on etch pit formation during dissolution and weathering. Pioneering work on dislocation theory by physicists and materials scientists conclusively demonstrated that if nucleation of etch pits on a perfect surface is to occur, it must first overcome a free energy barrier (Sangwal, 1987). In the case of pit development at dislocations, the occurrence and the magnitude of this energy barrier are controlled by solution saturation state and the strain energy and size of the dislocation cores (e.g., Frank, 1951; Cabrera et al., 1954; Cabrera and Levine, 1956; Gilman et al., 1960; Schaarwächter, 1965a, 1965b; Van der Hoek, 1982). Renewed application of the dislocation theory to mineral dissolution resulted in a 'phase diagram' that projected the controls of core size and saturation state on etch pit development (Lasaga, 1983; Lasaga and Blum, 1986). The same work also examined a variety of free energies associated with dislocation-controlled mineral dissolution reactions and showed that conditions in natural environments do not always satisfy the thermodynamic requirements for pit formation on major rock-forming minerals. Aside from the theoretical work and various concordant observations made on metals and simple ionic crystals such as LiF

* Author to whom correspondence should be addressed (hteng@gwu.edu).

and NaCl (Gilman et al., 1958; Johnston, 1962; Sangwal, 1987 and ref. therein), few experimental studies on minerals have been conducted. However, despite the general lack of experimental data, the controls of saturation state on mineral surface pitting are clearly demonstrated in Brantley et al. (1986). The laboratory results from this study showed no significant pit formation on quartz surfaces during hydrothermal dissolution until the saturation state fell below 75% of the equilibrium value. The fieldwork of this study revealed that surface pitting on quartz grains was controlled by the Si saturation level in pore water that varies with depth in soil profiles. These findings demonstrate that understanding the controls of saturation state is critical to formulate accurate rate laws for laboratory dissolution, and is also essential to fully understand the natural weathering processes.

The goals of the present study are (1) To apply the dislocation theory to calcite dissolution and obtain the theoretical critical undersaturation above which etch pits form at line dislocations; (2) To experimentally determine the critical undersaturation by monitoring the surface behavior of calcite $\{10\bar{1}4\}$ cleavage faces at various saturation states via in situ fluid cell Atomic Force Microscopy (AFM); and (3) To compare the theoretical predictions to the experimental observations. Findings from this study are discussed in reference to the dependence of dissolution mechanism upon saturation state. The geochemical significance of these results is discussed with regard to the relationships between dislocation density and dissolution kinetics and between chemical affinity and dissolution rate.

2. MATERIAL AND METHODS

2.1. Sample and Solution Preparation

Calcite $\{10\bar{1}4\}$ faces were obtained by using a razor blade to cleave a large crystal of optical-quality Iceland spar (Brazil). The cleaved fragments (approximately $2\times2\times0.5$ mm) were examined by optical microscopy to ensure the cleavage faces were free of cracks. A N_2 (g) burst was then applied to the targeted surface to remove any small adhering particles. Each fragment was mounted onto a cover-slip using sealing wax. The cover-slip was subsequently adhered to a magnetic steel puck using double-sided adhesive tape.

Stock solutions having a saturation index Ω of 1 ± 0.07 were prepared by dissolving 2.500×10^{-4} moles of $CaCl_2$ ($CaCl_2 \cdot H_2O$, Aldrich®, 99.99%) and 2.483×10^{-3} moles of sodium bicarbonate ($NaHCO_3$, Aldrich®, 99.99% +) into a liter of distilled, deionized water (resistance $\geq$ 18.8 megaohm-cm). Saturation index Ω is defined as the ratio of ionic activity product to solubility product. The value of solubility product used in this study was $10^{-8.48}$. The solutions were immediately sealed in volumetric flasks to prevent CO_2 degassing. A fresh stock solution was used every 8 to 10 h during the experiments to minimize the errors in estimating the experimental saturation states.

2.2. Solution Chemistry

Experimental solutions were made by incrementally diluting the stock solutions. Saturation states and chemical speciation of the experimental solutions were determined using the numerical code MINT-EQA2 (Allison et al., 1991). The AFM fluid cell and the input reservoir were assumed to approximate a closed system since CO_2 degassing was negligible due to the liquid-full environment. Aqueous complexes considered in the calculation were $CaCO_3^o$, $CaHCO_3^+$, $CaOH^+$, $NaCO_3^-$, $NaHCO_3^o$, HCO_3^-, and $H_2CO_3^o$. The Davies equation was used to calculate activity coefficients.

Experiment solutions had values of Ω = 0.843, 0.687, 0.541, 0.410, 0.294, 0.193, 0.111, 0.051, 0.012, and 0.007. The accumulated errors in these Ω values, which came from both the stock solutions and the

diluting procedure, were estimated to be approximately from 0.063 to 0.003. Ionic strengths of the experimental solutions extended from 10^{-3} to 10^{-5} molal and pH from 8.2 ~ 7.9.

2.3. AFM Imaging in Fluid Cell

In situ fluid cell imaging was conducted at Contact Mode® using a Nanoscope IIIa Scanning Probe Microscope (Digital Instruments) and a piezoelectric scanner with a maximum scan area of 120×120 μm. Commercially available oxide-sharpened Si_3N_4 probes were used for AFM imaging. These probes consist of V-shaped cantilevers that have lengths of 100 and 200 μm and force constants of approximately 0.06 to 0.12 Newton m^{-1}. The square pyramidal shaped lever tips have a radius of approximately 4–50 nm. Scan rates ranged from 3 to 8 Hz with 512 sampling points per scan line, corresponding to a capture time of 170 to 64 s per image, respectively. This translates to a tip velocity of 3 to 8 $\mu m/s$ on a 1×1 μm image. The contact force was optimized by tuning the force calibration curve to minimize tip induced surface damage (Park et al., 1996). The AFM instrument was usually powered on one to two hours before each experiment to reduce the thermal drift of the scanner during data collection (Henriksen and Stipp, 2002).

Each experiment began on a freshly prepared sample. The substrate surface was first imaged in air to locate a relatively flat area and to optimize image quality. A slightly undersaturated solution ($\Omega = ~$ 0.95) was then introduced into the AFM fluid cell to gently dissolve the topmost layer that might have been damaged by the cleaving process. During this process that usually lasted approximately 1–2 h, a fresh stock solution was made and ready to be diluted at specified proportions. After the removal of the topmost layer, an experimental solution was injected as a continuous flow into the fluid cell using a syringe pump. At each state of saturation, the surface was allowed to react with the solution for at lease 30 min. All images were collected with flow-through rates greater than 30 ml/hr to maintain the saturation state in the cell as close to that of the input solution as possible (Teng et al., 2000).

3. OBSERVATIONS

Freshly prepared surfaces exhibited flat terraces separated by steps. The steps had heights of small integer multiples of 3 $\pm$ 0.3 Å that corresponds to the thickness of a $(10\bar{1}4)$ monolayer. Upon injecting solutions with low undersaturations ($\Omega >$ 0.843), steps gradually began to retreat while terraces remained intact. This observation is most visible at narrow terraces with sharp corners that resulted from mis-cuts during sample preparation (Fig. 1, A&B). Dissolution continued to progress in this mode with saturation state decreasing from Ω = 0.843 to 0.541 (Fig. 1C). Repeated experiments on eight samples showed the development of the first visible etch pits at Ω = 0.541 and 0.410 (Fig. 2, A1, B1, and C1) within 3 to 30 min. Dissolution up to an additional 150 min showed no visible increase in pit density at these undersaturations; however, continuous dissolution at pit walls and step edges eventually consumed the early formed etch pits. Initial etch pit shapes were not readily identifiable due to limitations by image resolution. Nevertheless, grown pits clearly depicted the rhombic morphology that is consistent with observations of previous studies (Stipp et al., 1994; Liang et al., 1996; Teng et al., 1997).

Decreasing the saturation state from Ω = 0.540 ~ 0.410 to 0.012 led to a slow and noticeable increase in pit density (Figs. 2, 3, and 4A). Repeated experiments showed that each time a more undersaturated solution was introduced, the nucleated pits tended to form specific clusters rather than randomly distribute. This clustering phenomenon is best seen in Figure 2-C2 where pits are aligned along two bands that are parallel to each other but separated by approximately 15 microns. In addition, new
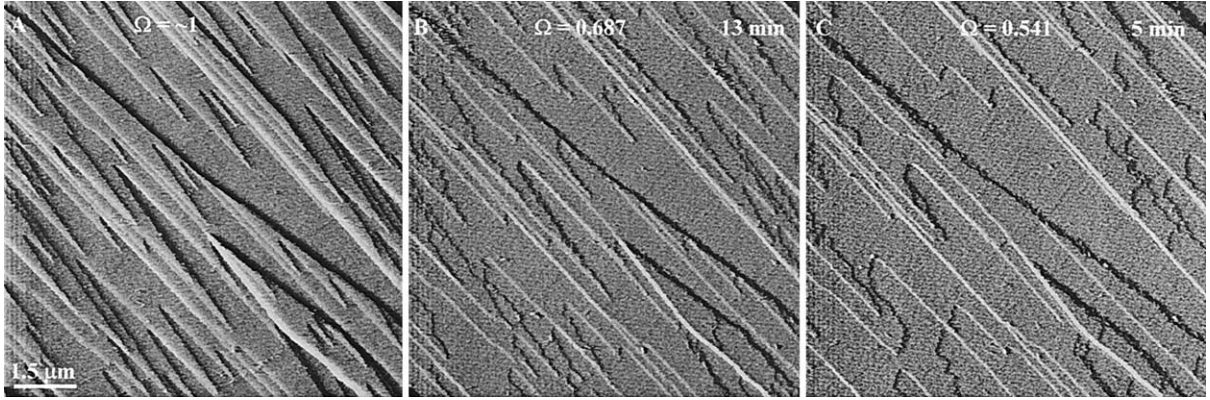
Fig. 1. In situ AFM images of a dissolving $\{10\bar{1}4\}$ surface in solutions with (A) $\Omega \approx 1$, (B) $\Omega = 0.687$, and (C) $\Omega = 0.541$ showing existing step-assisted dissolution. Notice the absence of etch pits on the dissolving surface under the experimental conditions.

pits formed at these saturation conditions were seldom seen to nucleate within existing ones.

A precipitous and abrupt leap in pit density took place when the saturation state was reduced to $\Omega = 0.007$ (Fig. 4, A & B), in sharp contrast to the slow and seemingly ordered fashion of pit formation at higher saturation states. Simultaneous pit formation was observed within two minute upon solution injection and new pits developed randomly on terraces and within existing pits. The steep change in pit density, which ranges from 2 to 3 orders of magnitude, is shown in Figure 5. A comparison of images taken in $\Omega = 0.007$ solution (Fig. 4B) and in distilled, deionized water (Fig. 4C) suggests that surface morphology and pit density remained largely unchanged despite further increases in undersaturation. Continuous dissolution of these samples showed that in $\Omega = 0.007$ solution and in distilled, deionized water, shallow pits considerably outnumbered deeper holes.

4. DISCUSSION

From the above AFM observations, it is clear that the saturation states of experimental solutions have a profound impact on if, when, and how many etch pits form. Therefore, further issues to be addressed concern whether or not these observations are predicted by the dislocation theory and the geochemical implications of the saturation controls on dissolution.

4.1. Critical Undersaturation for Pit Formation

Following the approaches of the dislocation theory (Cabrera et al., 1954; Cabrera and Levine, 1956), the free energy change upon nucleation of an etch pit at a line defect, ΔG_{pit}, may be expressed as

$$\Delta G_{pit} = (\pi r^2 h/\bar{v})\Delta\mu + (2\pi rh)\bar{\gamma} - (Khb^2/4\pi)\ln(r/r_o) \quad \text{(i)}$$

where r and h are the radius and the depth of the pit, $\bar{\gamma}$ and $\bar{v}$ are the average surface free energy (i.e., ignoring the crystal anisotropy) and the specific molecular volume of the solid, respectively; $\Delta\mu$ is the chemical potential of the solute; b is the modulus of the Burgers vector, and r_o is the core radius of the line defect. The magnitude of K depends on the dislocation

type: $K = G$ for screw dislocation where G stands for the shear modulus, and $K = G/(1-\vartheta)$ for edge dislocation where ϑ is the Poisson's ratio. The behavior of ΔG_{pit} with regard to r hinges upon the two solutions of the equation $d(\Delta G_{pit})/dr = 0$:

$$r_\pm = 1/2r_c[1 \pm \sqrt{1-(4r_F/r_c)}] \quad \text{(ii)}$$

where $r_c = -(\bar{\gamma}\bar{v})/\Delta\mu$ is the critical radius for two-dimensional nucleation (Cabrera et al., 1954) and $r_F = Kb^2/(8\pi^2\bar{\gamma})$ is the Frank radius (Frank, 1951). The critical radius gives the minimal size of the pit at a specific saturation state; for $r < r_c$, the pit is unstable and should disappear. The Frank radius defines the equilibrium size of the dislocation core; for $r < r_F$, the linear elasticity theory becomes invalid. Equation (ii) states that if $4r_F > r_c$, there is no real solution for r and, therefore, ΔG_{pit} decreases monotonically with increasing r, indicating spontaneous pit formation occurs. If $4r_F = r_c$, there is a single root, $r_+ = r_- = 1/2r_c$, implying the occurrence of a zero inflection point on the $\Delta G_{pit}(r)$ curve. When $4r_F < r_c$, there are two roots, corresponding to a maximum and a minimum ΔG_{pit}, signifying the pit formation is limited by a free energy barrier defined by the difference between the two extrema. This barrier, ΔG^*_{pit}, can be obtained by solving $[\Delta G_{pit}(r_+) - \Delta G_{pit}(r_-)]$ after inserting Eqn. (ii) into Eqn. (i):

$$\Delta G^*_{pit} = \frac{Khb^2}{4\pi}\ln\left(\frac{1-[1-4r_F/r_c]^{1/2}}{1+[1-4r_F/r_c]^{1/2}}\right) + \frac{\pi h\bar{\gamma}^2\bar{v}}{\Delta\mu}\sqrt{\left(1-\frac{4r_F}{r_c}\right)}.$$

(iii)

In the absence of defects, the following simpler expression for ΔG^*_{pit} can be derived after omitting the third item on the right side of Eqn. (i):

$$\Delta G^*_{pit} = -\pi h\bar{v}\bar{\gamma}^2/\Delta\mu. \quad \text{(iv)}$$

Inspection of Eqn. (iii) reveals that $\Delta G^*_{pit} \to 0$ when $4r_F/r_c \to 1$. Because r_c is a function of $\Delta\mu$, there must exist a critical chemical potential, $\Delta\mu_c$, at which $4r_F/r_c = 1$ so that $\Delta G^*_{pit} = 0$ and etch pits form spontaneously. The critical chemical potential is found to be (Cabrera and Levine, 1956)
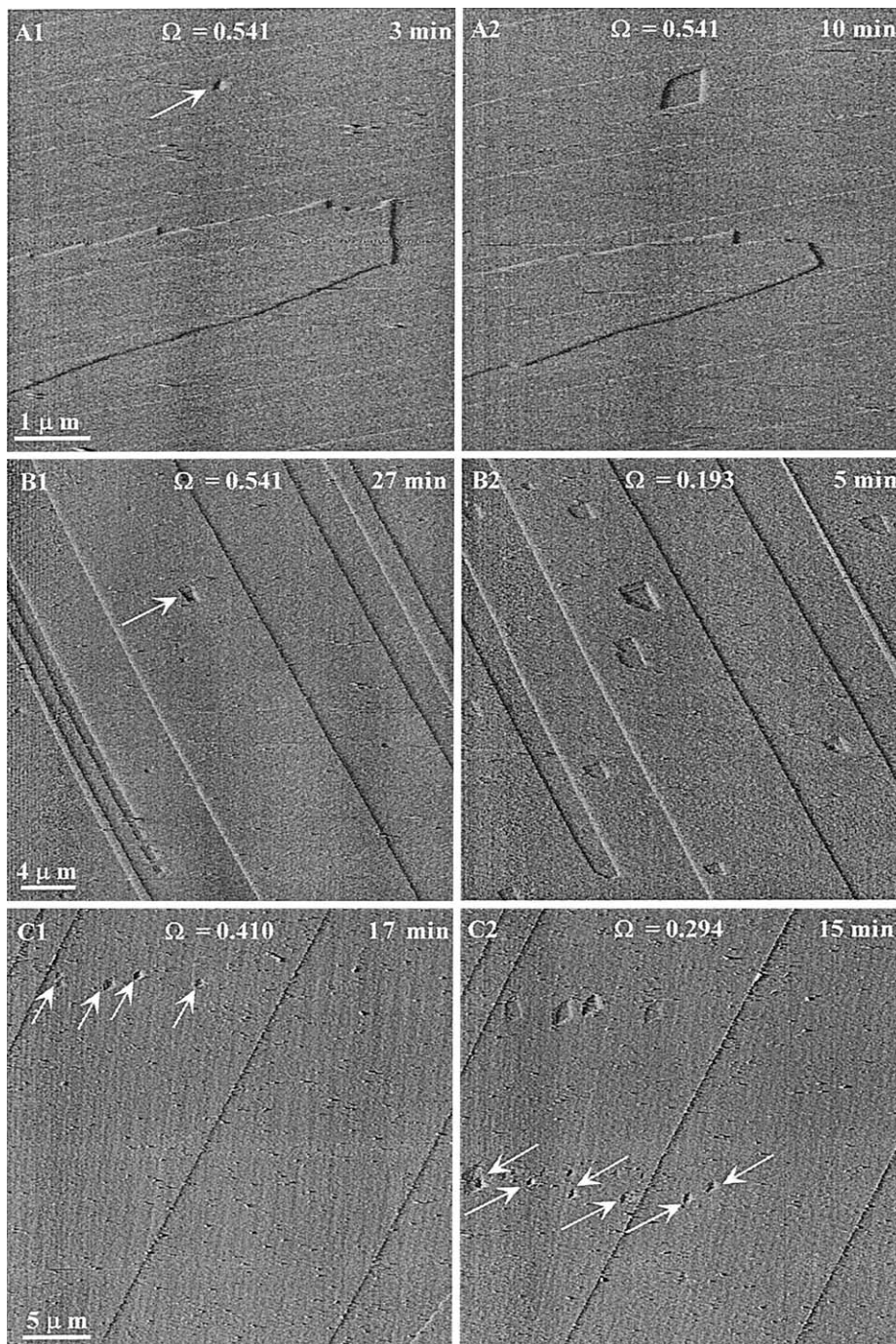
Fig. 2. In situ AFM images of dissolving {10$\bar{1}$4} surfaces at 0.541 > Ω > 0.193. Images (A1)/(A2) show the growth of an etch pit at Ω = 0.541. Images (B1)/(B2) and (C1)/(C2) show the gradual increase of visible etch pits in the imaging area with increasing undersaturations. Arrows point to the etch pits at their first glance.

$$\Delta\mu_c = -\frac{2\pi^2\bar{\gamma}^2\bar{v}}{Kb^2} \qquad (v)$$

after solving $r_c = 4r_F$. Hence, Eqn. (iii) predicts the existence of an energy barrier for pit formation at line dislocations unless the value of $\Delta\mu$ satisfies the relationship $r_c = 4r_F$. On the other hand, Eqn. (iv) outlines an asymptotic dependence of energy

barriers upon $\Delta\mu$ and indicates that an energy barrier is always present for pit formation on defect-free surfaces.

Following the definition

$$\Delta\mu = K_bT\ln(\Omega) \qquad (vi)$$

where k_b is the Boltzmann constant, and T the temperature (298 K in this study), the $\Delta G^*_{pit}(\Delta\mu)$ curves on calcite {10$\bar{1}$4} faces
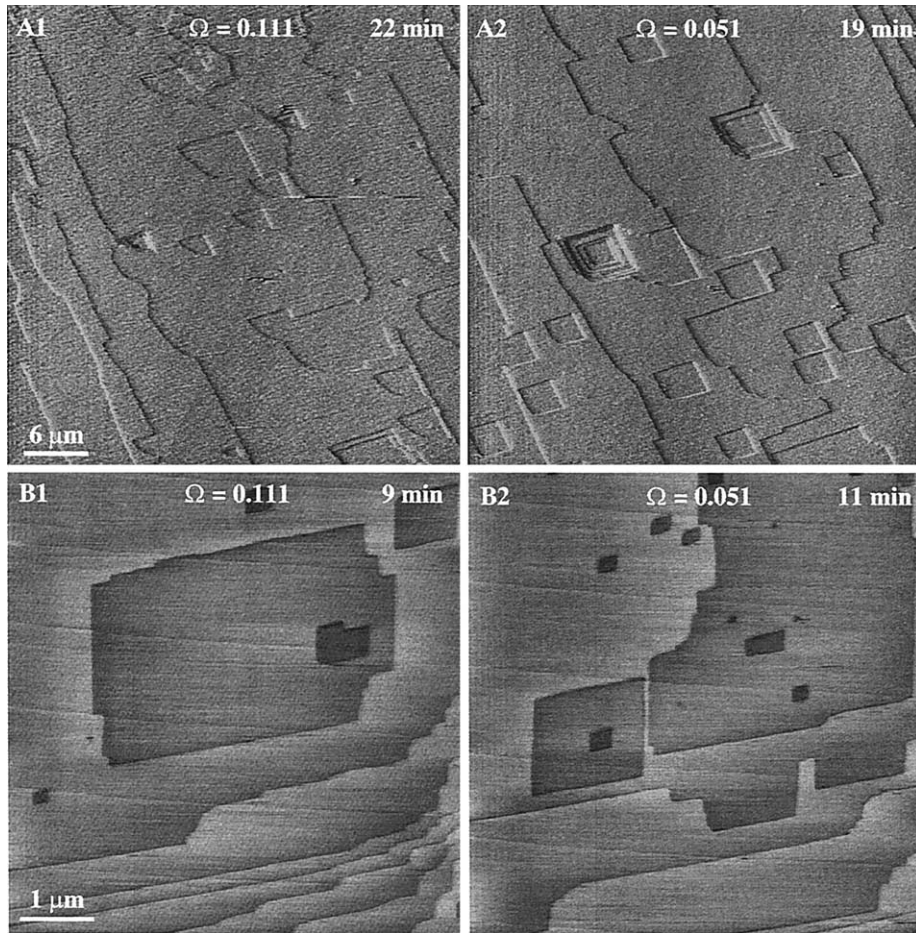
Fig. 3. In situ AFM images of dissolving $\{10\bar{1}4\}$ surfaces at $\Omega = 0.111$ and 0.051 showing the slow changes in surface morphologies.

are calculated for the formation of a monolayer deep etch pit at a non-defect site, a screw dislocation, and an edge dislocation (Fig. 6). Other values used in the calculation are $\bar{\gamma} = 94$ mJ/m^2 (Christofferson et al., 1988), $\bar{v} = 6.123 \times 10^{-23}$ cm^3 (computed from the calcite density of 2.71 g/cm^3), $G = 32 \times 10^9$ Pa

(Mavko et al., 1998), $\vartheta = 0.32$ (Mavko et al., 1998), and b is assumed to be 0.3 nm, the thickness of an individual $(10\bar{1}4)$ plane. Calculated critical saturation states are $\Delta\mu_c = -276.91 \times 10^{-23}$ J and -403.36×10^{-23} J, or $\Omega_c = 0.513$ and 0.375, for edge and screw dislocations, respectively (Fig. 6).
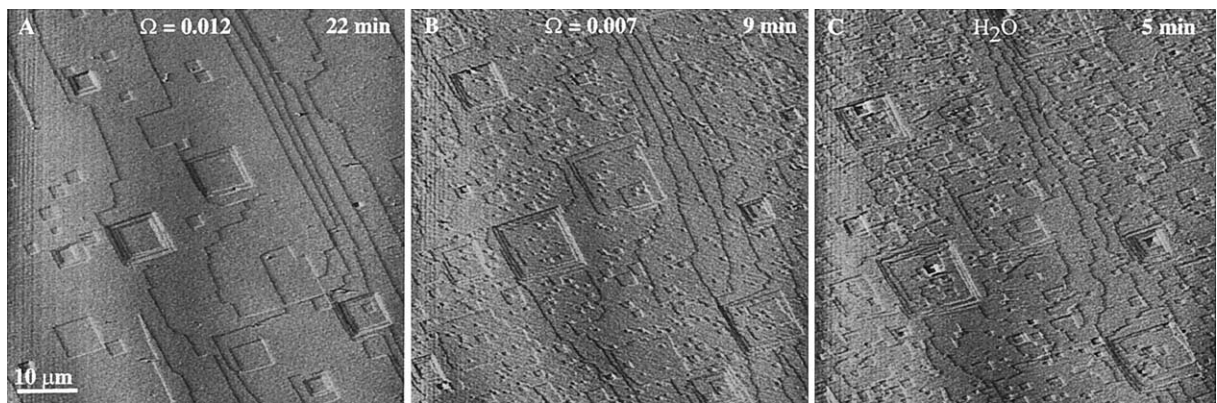

Fig. 4. In situ AFM images of a dissolving $\{10\bar{1}4\}$ surface showing the abrupt leap in pit density when the saturation index decreases from (A) $\Omega = 0.012$ to (B) $\Omega = 0.007$ and the resemblance of the surface morphologies at (B) $\Omega = 0.007$ and in (C) distilled, deionized water.
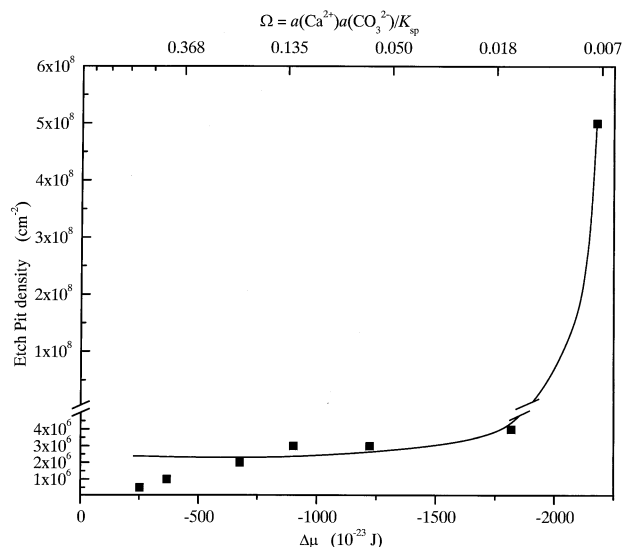
Fig. 5. Measured pit densities against solution undersaturations showing the sudden rise of pit density at far from equilibrium. The solid squares are the measurements and the dashed line is an exponential fit to the data. Notice that no pits are observed at $\Omega > \sim 0.54$ or $\Delta\mu > -250 \times 10^{-23}$ J and pit density slowly increases with increasing undersaturation until Ω reaches ~ 0.01 or $\Delta\mu \sim -2000 \times 10^{-23}$ J.

Examination of Figure 6 yields the following predictions:

1. At close to equilibrium ($\Delta\mu > \sim -100 \times 10^{-23}$ J or $\Omega > \sim 0.78$), etch pit nucleation is highly energetically unfavorable.

2. At mild undersaturations ($\Delta\mu \approx -275 \times 10^{-23}$ J or $\Omega \approx 0.50$), the nucleation barrier at edge dislocations disappears, indicating the beginning of pit formation at line defects.
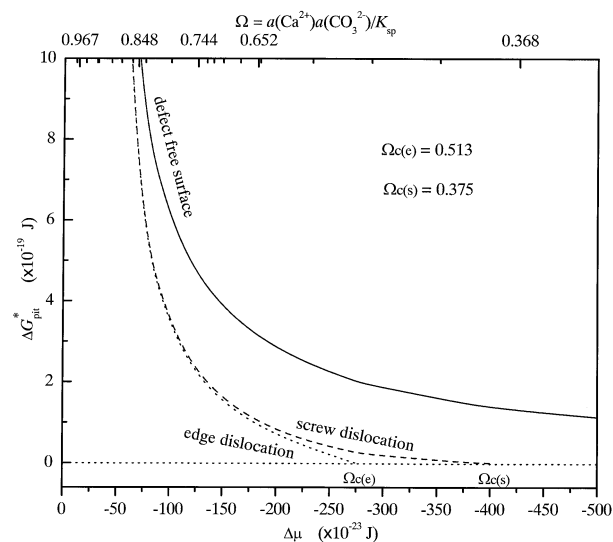

Fig. 6. Dependence of nucleation barriers upon chemical potential (bottom x-axis) and saturation index (top x-axis). The values of ΔG^*_{pit} are determined by using Eqn. (iii) for edge and screw dislocations and Eqn. (iv) for defect free surfaces. The values of critical undersaturations, $\Omega_{c(e)}$ and $\Omega_{c(s)}$, at which the barriers vanish for pit nucleation at edge and screw dislocations, respectively, are calculated using Eqn. (v).

3. Screw dislocations become active when saturation index decreases to ~ 0.37 or $\Delta\mu = \sim -400 \times 10^{-23}$ J.

These predictions appear to be consistent with the experimental observations: no etch pits were observed at near equilibrium conditions and the first appearance of surface pitting occurred when Ω was reduced to $0.541 - 0.410$ (which corresponds to $\Delta\mu = -252.64 \times 10^{-23} - 366.66 \times 10^{-23}$ J). Although the image resolution did not allow for a clear identification of the types of dislocations that assisted in pit formation, the solution saturation states at which etch pits started to form are in good agreement with the predicted critical undersaturations of 0.510 to 0.375 for edge and screw dislocations, respectively.

A closer look at the theoretical and experimental results reveals that the observed critical saturation states are higher than the predicted values. This difference may be attributed to several factors. First, errors may have been introduced by the uncertainties in the Burgers vectors. The ΔG^*_{pit} ($\Delta\mu$) curve and the theoretical values of Ω_c were determined by assuming $b = 0.3$ nm for pure screw and edge dislocations. In reality, the value of b may vary considerably from sample to sample with a great deal of unpredictability. For example, Teng et al. (2000) showed that the modulus of the net apparent Burgers vectors in the calcite crystals collected from Chihuahua, Mexico, ranges from $\sim 0.3 - \sim 0.9$ nm. Because of the inherent inaccuracy in assuming a Burgers vector to be 0.3 nm, the b value used in the calculation may not truthfully reflect the actual size of the Burgers vectors in samples used in the experiments. Due to the inverse exponential dependence of $\Delta\mu_c$ upon b (Eqn. v), even a small deviation of the assumed b value from reality can produce a substantial discrepancy between the theoretical and the experimental values of $\Delta\mu_c$ and Ω_c. Additional errors can occur if the dislocations concerned in experiments have a mixed edge and screw character. In this case (which is in all likelihood a more realistic scenario), not only is the value of b poorly constrained, the calculation of the total elastic energy has to take into account the geometric relationship between the edge and the screw components (Hull and Bacon, 1997). In this study, the difference between the observed and the estimated critical undersaturations can be fully justified solely by the size of b if the assumed value is 20% larger than the monolayer thickness of 0.3 nm.

A second contribution to the difference may have come from approximating the anisotropic elastic field using the isotropic elasticity theory. More specifically, errors may exist in the calculated $\Delta\mu_c$ and Ω_c due to using bulk values of shear modulus and surface free energy to approximate the direction-specific ones that are largely unavailable. Using numerical calculation, Heinisch et al. (1975) estimated the elastic stress fields of several anisotropic minerals through the anisotropic elasticity theory and compared the results with the isotropic elastic solutions. Their findings indicated that although the moderate anisotropies of orthorhombic minerals, such as olivine and orthopyroxene, lead to a maximum of 20% difference in the elastic properties estimated by isotropic and anisotropic theories, the larger anisotropies in hexagonal minerals, calcite in particular, cause a substantial disparity. For example, the values of K (ref. Eqn. i) along different directions in calcite vary by as much as 220% for screw dislocations and 170% for

edge dislocations. The large anisotropy in calcite is also reflected by the surface energetics. Using measurements from spiral growth and the Gibbs-Thomson relationship, Teng et al. (1998) showed that the step energies along the $<\bar{4}41>_+$ and $<\bar{4}41>_-$ directions differ by about 28%. These findings suggest that the theoretical values of critical undersaturation obtained by neglecting crystal anisotropy should be used with caution because they contain unspecified uncertainties.

A third factor to be evaluated is the effect of dislocation core on etch pit formation. Neglecting the existence of dislocation cores in this study is not intended to belittle their importance, but instead is due to the difficulty in formulating and incorporating the core energy into calculations. Although it is generally agreed that core energy is only a small fraction of the total strain energy of a dislocation (e.g., <6%, Blum et al., 1990), different opinions do exist. For example, after studying pit formation on surfaces of metals and ionic/covalent crystals, Gilman (1960) proposed that the dislocation core energy is responsible for the nucleation of etch pits. His arguments are based upon the following reasoning:

1. It is much more difficult to form etch pits on metal surfaces than on ionic and covalent crystal faces. Conformably, the core energies of dislocations in metals are much smaller than those in other types of materials, while the dislocation elastic strain energies are similar in all materials.
2. The elastic stress fields tend to cancel out when dislocations are close to each other. Hence, etch pits should form faster at isolated dislocations than at clustered ones if elastic strain energy is responsible for pit formation. Yet, all dislocations etch at approximately the same rate.

Similar emphasis on the importance of core energy can also be found in Schaarwächter (1965a, 1965b), where the author proposed that etch pit formation can be initiated by different components of the overall strain energy. The core energy will be the dominant component unless a special condition where $r_F/r_o < 1/2$ is satisfied. Details of the specific effect of dislocation cores are beyond the scope of this study, but it should be pointed out that the errors in the calculated $\Delta\mu_c$ and Ω_c due to neglecting the core energy in this investigation are undetermined.

4.2. Defect-Assisted and Surface Nucleation-Induced Pit Formation

The marked increase in pit density seen at $\Omega < \sim 0.007$ apparently indicates the onset of a different cause in triggering pit formation. One of the following scenarios may represent this cause: (1) new types of defects become active; (2) two-dimensional surface nucleation (Burton et al., 1951) becomes operative, i.e., pits start to form in defect free areas. It is possible that the sharp rise in pit density at $\Omega < \sim 0.007$ resulted from point defect-induced pit formation, provided that the point defects had smaller strain energies than the line defects. However, given the experimental observations of several orders of magnitude increase in pit density (Fig. 5), the population of point defects must be significantly higher than that of the line defects for this explanation to be feasible. At room temperature, the concentration of point defects in MX type of ionic crystals is estimated to be on the order of 10^4–

$10^5/cm^3$ (Tilley, 1987). Metals have a somewhat higher point defect population; calculated concentrations of vacancies at melting points show that the defect population can reach as high as ~1% of the total atomic positions but decreases more than 15 orders of magnitude when the temperature is reduced to 300 K (Kraftmakher and Strelkov, 1970; Hull and Bacon, 1997). These concentration values translate into a maximum point defect density of about $1/cm^2$ assuming a monolayer thickness of 3Å, as for that of calcite $\{10\bar{1}4\}$ faces. Comparing the measured pit density of $\sim10^8/cm^2$ at $\Omega < \sim 0.007$ (Fig. 5), it is clear that point defects cannot be responsible for the pit density surge. What's more, if the rapid increase in pit density indicates the beginning of pit formation at point defects, continuous increase in undersaturation beyond ~ 0.007 should bring another discrete rise of pit density corresponding to the inception of two-dimensional surface nucleation. However, even upon the input of distilled, de-ionized water, no such increase was observed. This further supports the notion that the abrupt increase in pit density was not the results of point defect-induced pit formation.

Assuming defect-assisted pit formation is the primary dissolution mode between $\sim 0.007 < \Omega < 0.54$, we are left with a two-dimensional surface nucleation mechanism as the most likely cause for the sudden rise in pit density at $\Omega < \sim 0.007$. Two lines of reasoning support this notion. To begin, no significant changes in surface morphology or pit density were observed between the experiments at $\Omega = \sim 0.007$ and the experiments in distilled, deionized water (Fig. 4, B & C). According to Eqn. (iv), the energy barrier for unassisted pit nucleation will eventually become negligible when $|\Delta\mu|$ is sufficiently large. This thermodynamic condition should be adequately satisfied by distilled, deionized water. Hence, it would be a logical consequence that two-dimensional surface nucleation controls pit formation in experiments conducted in distilled, deionized water or solutions where the saturation state is not controlled. This inference is supported by MacInnis and Brantley (1992) where, in a study conducted using KCl solution, the authors reported a pit density of $10^5/cm^2$ on calcite crystals with a known dislocation density of $\sim 10^3/cm^2$. They suggested that the dissolution at a large number of non-dislocation sites may indicate spontaneous pit formation on perfect calcite surfaces. If it is to be believed that etch pit density reaches its maximal value when dissolution occurs through unassisted pit nucleation, then the insignificant change in pit density from $\Omega = 0.007$ to distilled, deionized water suggests that the maximum has been reached at $\Omega = 0.007$. This implies that unassisted pit nucleation has become operative at this saturation state.

A second supporting argument comes from a comparison of the estimated free energy barrier at $\Omega = 0.007$ and the melting enthalpy, ΔH_m, of calcite. For a first order approximation, the energy required to form an etch pit on a defect free surface and the melting enthalpy of the material should be about the same order of magnitude. To the best of my knowledge, there is no published ΔH_m data for calcite. However, using the classic relationship between solid-liquid interfacial energy and melting enthalpy, $\gamma^{SL} \cong 0.45\Delta H_m$, given by Turnbull and Cech (see Howe, 1997 and ref. therein), ΔH_m is calculated to be 0.32×10^{-19} J when $\gamma^{SL} = 94$ mJ/m^2 (Christofferson et al., 1988) and molecular volume is 6.13×10^{-23} cm^3. This value is

fairly close to the energy barrier of 0.25×10^{-19} J at $\Omega = 0.007$, which is estimated by using Eqn. (iv). The close proximity between ΔH_m and ΔG^*_{pit} implies that the energy released from dissolution-induced chemical bond disassociation may be sufficient enough for the system to offset the energy barrier for etch pit formation at non-dislocation sites. Thus, it is conceivable that unassisted pit nucleation starts to become active when the saturation state decreases to approximately 0.007.

4.3. Dependence of Dissolution Mechanism on Undersaturation and its Geochemical Implications

The observations that etch pits do not develop near equilibrium but form rapidly far from equilibrium suggest that dissolution occurs by means of three mechanisms. When $\Omega > 0.410-0.541$, dissolution at existing steps is the primary mechanism; when undersaturation falls in between $0.410-0.541$ to 0.007, both step-induced and defect-assisted dissolution are active; finally when undersaturation drops below 0.007, a new mechanism, unassisted and spontaneous two-dimensional pit nucleation, starts to play a dominant role and the effect of dislocation on dissolution becomes secondary. If we define the saturation state at which unassisted pit formation develops as Ω_{max}, the transition in dissolution mechanisms then hinges upon two critical saturation states, namely, Ω_c (given by Eqn. v) and Ω_{max}.

Two geochemical implications emerge from the presence of Ω_c and Ω_{max} during dissolution. First, it helps to understand the dependence of dissolution kinetics upon dislocation density. Numerous studies have documented that dislocation density has an insignificant effect on laboratory dissolution rates. For example, Brantley et al. (1986a) reported that presumed differences in dislocation etch pit density in calcite and fluorite show little effect on the dissolution kinetics of these minerals. Murphy (1989) found no difference in sanidine dissolution rate when dislocation density increased from $\sim 10^6$ to $10^8 - 10^9$ cm^{-2}. Blum et al. (1990) also noticed the insensitivity of dissolution kinetics to dislocation density when quartz was dissolved in distilled water and HF solutions; despite a more than 5 orders of magnitude increase in dislocation density, dissolution rate remained the same. Holdren et al. (1988) observed that the dissolution rate of calcic plagioclase was only three times greater when the dislocation density increased from $\sim 10^6$ to 10^9 cm^{-2}. A similar increase in dissolution kinetics was observed by Casey et al. (1988) in rutile for a dislocation density of $\sim 10^6$ to 4×10^{10} cm^{-2} and by Schott et al. (1989) in calcite for a dislocation density of $< 10^6$ to 10^9 cm^{-2}. If mineral dissolution is controlled by etch pit formation, as is suggested by various prior studies, the question then becomes: why does the increase in dislocation density, and therefore, the increased susceptibility to pit formation, not proportionally increase the dislocation rate?

A common approach in laboratory studies of mineral dissolution is to ignore the dependence of dissolution on saturation state by directly carrying out experiments in distilled water or solutions only with controlled acidity or ionic strength. This implies that dissolution in question is often occurring at far-from equilibrium conditions. It is therefore reasonable to assume that the saturation states in studies conducted under these conditions are below the corresponding Ω_{max} values of the minerals concerned. Hence, unassisted pit nucleation is probably playing a dominant role in controlling the dissolution kinetics and any increase in dissolution rates resulting from a dislocation density increase will be overwhelmed by the spontaneous pit formation on the dissolving surfaces. Almost all the studies previously mentioned, that reported a weak, if existent, dependence of dissolution rate on dislocation density, were conducted in solutions with uncontrolled saturation states. It is therefore likely that experimental conditions in these studies were such that $\Omega < \Omega_{max}$ and two-dimensional pit nucleation controlled the dissolution kinetics. This explanation is consistent with Blum et al. (1990) and MacInnis and Brantley (1992) who both suggested that pit formation in defect free regions in highly undersaturated solutions provides an extra step source that overwhelms the contributions of dislocations to dissolution rate.

While the presence of Ω_{max} explains the insignificance of dislocation density with respect to dissolution kinetics at conditions extremely far from equilibrium, the occurrence of Ω_c also predicts that dissolution rate has a weak dependence on dislocation density at conditions close to equilibrium, i.e., when $\Omega > \Omega_c$. This is because the energy barriers at $\Omega > \Omega_c$ are still present and etch pits cannot spontaneously form at dislocations. Consequently, the number of dislocations will have little bearing on dissolution rate.

Furthermore, the controls of Ω_c and Ω_{max} on etch pit formation suggest that the strongest effect of dislocation density on dissolution kinetics should occur in solutions with $\Omega_{max} < \Omega < \Omega_c$. This seems to contradict the supposition by Blum et al. (1990) that dislocation density will have a stronger effect on dissolution kinetics at near-equilibrium conditions. However, the apparent contradiction can be resolved if the dislocations in question have large Burgers vectors. In this scenario, the values of Ω_c can be very close to equilibrium because the critical undersaturation is exponentially related to the inverse of the Burgers vectors (ref. Eqn. v).

The second geochemical implication is that dissolution rate should not exhibit a linear dependence upon solution saturation state. This may provide additional insight into the complex relationship between dissolution rate R and free energy of dissolution reactions ΔG. Several studies in the past decade reported that the $R(\Delta G)$ curve is characterized by a steeper slope bordered by two 'plateaus'. For example, Nagy and Lasaga (1992) observed that gibbsite dissolution rate shows a markedly weak dependence on free energy when ΔG is greater than -0.5 to -0.2 kcal mol^{-1} and smaller than ~ -1.1 kcal mol^{-1}; between the two plateaus the dissolution rate quickly decreases as the saturation state moves toward the equilibrium state. The same phenomenon is also observed in other minerals, including albite, labradorite, and smectite, although the ΔG range where plateaus occur differs for each mineral (Lasaga and Luttge, 2001). The saturation controlled changes in dissolution mode reported in the present study qualitatively match the $R(\Delta G)$ behavior found in these previous studies. At far from equilibrium when $\Omega < \Omega_{max}$, no new steps can be exposed and dissolution rate is capped by the maximum number of steps; at close to equilibrium when $\Omega > \Omega_c$, very little pit formation occurs and dissolution is limited by the number of existing steps; when $\Omega_{max} < \Omega < \Omega_c$, increasing undersaturation increases pit density and therefore the number of steps to yield a

meaningful dependence of R on ΔG. It is therefore reasonable to conclude that dissolution rate obtained at $\Omega < \Omega_c$ conditions cannot be applied to conditions where $\Omega > \Omega_c$ using a linear relationship. Significant errors can occur if laboratory dissolution rates are applied to natural systems without considering the effects of Ω_c and Ω_{max} or if measurements taken at extremely far from equilibrium conditions are used to model natural weathering processes that are often close to equilibrium.

Lasaga and Luttge (2001) correctly incorporated the impact of Ω_c on etch pit formation into a dissolution rate law based on a step wave model. The proposed rate expression approaches the form of $A(1 - e^{\alpha \frac{\Delta G}{RT}})$ at far from equilibrium conditions (A and α are constants), which is consistent with the conclusions drawn from the transition state theory. However, the step wave model gives no clear indication on how and when unassisted pit nucleation begins to control the dissolution kinetics. In this regard, a 'general' dissolution rate law remains to be developed.

Although the observations in this study were made on calcite, the above discussion should be applicable to the general scenario of dissolution, since the existence of Ω_c is theoretically predicted and experimentally verified (e.g., Frank, 1951; Cabrera et al., 1954; Cabrera and Levine, 1956; Gilman et al., 1960; Schaarwächter W., 1965a, 1965b; Van der Hoek, 1982; Lasaga and Blum, 1986; Brantley et al., 1986; Blum et al., 1990; Lasaga and Luttge, 2001). The significance of Ω_{max} has not been addressed extensively in the literature; however, the occurrence of this important threshold is implied by dissolution thermodynamics (Eqn. iv). The next important step in examining the effects of saturation state on dissolution kinetics is to repeat the above experiments on other minerals, determine the corresponding values of Ω_c and Ω_{max}, and then evaluate the impact of the two critical saturation states on bulk dissolution rates. Results of such studies will put more constraints in developing geochemical rate laws describing weathering and cycling of elements at various scales.

5. SUMMARY

Surface behavior of calcite $\{10\bar{1}4\}$ faces was studied under conditions where saturation state was incrementally decreased during dissolution. Three dissolution modes were observed: above a critical undersaturation $\Omega_c = 0.541–0.410$, no surface pitting was developed and dissolution visibly occurred at existing steps; in the range from $\Omega = \Omega_c$ to $\Omega = \sim 0.007$, etch pits formed and pit density gradually increased with increasing undersaturation; finally when undersaturation fell below another critical value of $\Omega_{max} = 0.007$, a precipitous increase in pit density took place. The values of Ω_c came in good agreement with the predictions of the dislocation theory. The occurrence of Ω_{max} is not directly predicted but nevertheless is a logical consequence of dissolution thermodynamics. Estimated energy barrier for pit formation at defect free sites at $\Omega = \Omega_{max}$ is close to the projected melting enthalpy of calcite, suggesting that spontaneous pit nucleation may have taken place at this saturation state. These observations are explained as two-dimensional surface nucleation controlled dissolution when $\Omega < \Omega_{max}$, and defect assisted dissolution in between Ω_{max} and Ω_c.

These findings have important geochemical significance. To begin, they predict that dissolution at far from equilibrium (Ω

$< \Omega_{max}$) conditions is not controlled by dislocations, therefore, dissolution kinetics should not, or should only weakly, depend on dislocation density. This is strongly supported by earlier experimental observations. Secondly, they imply that dislocation density should have the strongest effect on dissolution rate when Ω sits in between Ω_{max} and Ω_c, as opposed to at near equilibrium conditions ($\Omega > \Omega_c$) as suggested by earlier studies. Thirdly, they establish a framework to justify the non-linear dependence of dissolution rate on free energy of dissolution reactions. The significant increase in pit density at $\Omega \sim \Omega_{max}$ is not indicated by the current expressions of dissolution rate equations. As such, it is suggested that a 'general' rate law remains to be developed to describe the overall dissolution processes.

REFERENCES

Allison J. D., Brown D. S., and Nove-Gradac K. J. (1991) MINTEQA2/PRODEFA2, A geochemical assessment model for environmental systems: Version 3.0 User's Manual, US Environmental Protection Agency, Athens, GA.

Berner R. A. (1981) Kinetics of weathering and diagenesis. *Rev. Mineral.* **8,** 111–134.

Berner R. A., Lasaga A. C., and Garrels R. M. (1983) The carbonate-silicate geochemical cycle and its effect on atmospheric carbon dioxide over the past 100 million years. *Am. J. Sci.* **283,** 641–683.

Blum A. E., Yund R. A., and Lasaga A. C. (1990) The effect of dislocation density on the dissolution rate of quartz. *Geochim. Cosmochim. Acta* **54,** 283–297.

Brady P. V. and W. A. House. (1995) Surface-controlled dissolution and growth of minerals. In *Physics and Chemistry of Mineral Surfaces* (ed. P. V. Brady), CRC Press.

Brantley S. L. and Chen Y. (1995) Chemical weathering rates of pyroxenes and amphiboles. *Rev. Mineral.* **31,** 119–168.

Brantley S. L., Crane S. R., Crerar D. A., Hellmann R., and Stallard R. (1986) Dissolution at dislocation etch pits in quarts. *Geochim. Cosmochim. Acta* **50,** 2349–2361.

Brantley S. L., Crane S. R., Crerar D. A., Hellmann R., and Stallard R. (1986a) Dissolution etch pits in quarts. In *Geochemical Processes at Mineral Surfaces* (eds. J. A. David and K. F. Hayes) pp 633–649. American Chemical Society DC.

Burton W. K., Cabrera N., and Frank F. C. (1951) The growth of crystals and the equilibrium structure of their surfaces. *Royal Soc. London Philos. Trans.* **A243,** 299–358.

Cabrera N. and Levine M. M. (1956) On the dislocation theory of evaporation of crystals. *Phil. Mag.* **1,** 450–458.

Cabrera N., Levine M. M., and Plaskett J S. (1954) Hollow dislocations and etch pits. *Phys. Rev.* **96,** 1153.

Casey W. C., Carr M. J., and Graham R. A. (1988) Crystal defects and the dissolution kinetics of rutile. *Geochim. Cosmochim. Acta* **52,** 1545–1556.

Christofferson J., Christofferson M. R., Kibalczyc W., and Perdok W. G. (1988) Kinetics of dissolution and growth of calcium fluoride and effects of phosphate. *Acta Odontol Scand.* **46,** 325–336.

Frank F. C. (1951) Capillary equilibria of dislocated crystals. *Acta Cryst.* **4,** 497–501.

Garrels R. M. and Mackenzie F. T. (1971) Evolution of sedimentary rock. Norton, New York.

Gilman J. J. (1960) Discussion to "Etching of metals and semiconductors" by J. W. Faust. In *The surface chemistry of metals and semiconductors* (ed. H. C. Gatos), pp 172–173. Wiley, New York.

Gilman J. J., Johnston W. G., and Sears G. W. (1958) Dislocation etch pit formation in lithium fluoride. *J. Appl. Phys.* **29,** 747–754.

Gratz A. J., Bird P., and Quiro G. B. (1990) Dissolution of quartz in aqueous basic solution, 106–236 °C: Surface kinetics of "perfect" crystallographic faces. *Geochim. Cosmochim. Acta* **54,** 2911–2922.

Gratz A. J., Manne S., and Hansma P. K. (1991) Atomic force microscopy of atomic-scale ledges and etch pits formed during dissolution of quartz. *Science* **251,** 1343–1346.

Hegleson H. C., Murphy W. M., and Aagaard P. (1984) Thermodynamic and kinetic constrains on reaction rates among minerals and aqueous solution. II. Rate constants, effective surface area, and the hydrolysis of feldspar. *Geochim. Cosmochim. Acta* **48,** 2405–2432.

Heinisch H. L. Jr, Sines G., and Goodman J. W. (1975) Elastic stresses and selfenergies of dislocations of arbitrary orientation in anisotropic media: olivine, orthopyroxene, calcite and, quartz. *J. Geoph. Res.* **80,** 1885–1896.

Henriksen K. and Stipp S. L. S. (2002) Image distortion in scanning probe microscopy. *Am. Min.* **87,** 5–16.

Hillner P. E., Manne S., Gratz A. J., and Hansma P. K. (1992) AFM images of dissolution and growth on a calcite crystal. *Ultramicros.* **42-44,** 1387–1393.

Holdren G. R., Casey W. H., Westrich H. R., Carr M., and Boslough M. (1988) Bulk dislocation densities and dissolution rates in a calcic plagioclase. *Chem. Geol.* **70,** 79.

Holdren G. R. Jr. and Berner R. A. (1979) Mechanism of feldspar weathering—I. Experimental studies. *Geochim. Cosmochim. Acta* **43,** 1161–1171.

Howe J. M. (1997) Interfaces in materials. Wiley, New York.

Hull D. and Bacon D. J. (1997) Introduction to dislocations (3rd edn.) Butterworth-Heinemann, Oxford.

Johnston W. G. (1962) Dislocation etch pits in nonmetallic crystals. In *Prog. Ceramic Sci.,* (ed. J. E. Burke) v2, pp 3–75. Pergamon Press, Oxford.

Kraftmakher Y. A. and Strelkovn P. G. (1970) Equilibrium concentration of vacancies in metals. In *Vacancies and interstitials in metals* (eds. A. Seeger, D. Schumacher, W. Schilling, and J. Diehl) pp 59–79. North-Holland Pub. Co., Amsterdam.

Lasaga A. C. (1983) Kinetics of silicate dissolution. In *4th international symposium on water-rock interactions,* pp. 269–274. Misasa, Japan.

Lasaga A. C. and Blum A. E. (1986) Surface chemistry, etch pits and mineral water reactions. *Geochim. Cosmochim. Acta* **50,** 2363–2379.

Lasaga A. C. and Luttge A. (2001) Variation of crystal dissolution rate based on a dissolution stepwave model. *Science* **291,** 2400–2404.

Lasaga A. C., Soler J. M., Ganor J., Burch T. E., and Nagy K. L. (1994) Chemical weathering rate laws and global geochemical cycles. *Geochim. Cosmochim. Acta* **58,** 2361–2368.

Lee M. R. and Parsons I. (1995) Microstructural controls of the weathering of perthitic alkali feldspars. *Geochim. Cosmochim. Acta* **59,** 4465–4488.

Liang Y., Baer D. R., McCoy J. M., Amonette J. E., and LaFemina J. P. (1996) Dissolution kinetics at the calcite-water interface. *Geochim. Cosmochim. Acta* **60,** 4883–4887.

MacInnis I. N. and Braneley S. L. (1992) The role of dislocations and surface morphology in calcite dissolution. *Geochim. Cosmochim. Acta* **56,** 1113–1126.

Mavko G., Mukerji R., and Dvorkin J. (1998) The rock physics handbook. Cambridge Uni. Press, New York.

Murphy W. M. (1989) Dislocation and feldspar dissolution: theory and experimental data. *Chem. Geol.* **70,** 163.

Nagy K. L. and Lasaga A. C. (1992) Dissolution and precipitation kinetics of gibbsite at 80° and pH 3: The dependence on solution saturation state. *Geochim. Cosmochim. Acta* **56,** 3093–3111.

Nugent M. A., Brantley S. L., Pantano C. G., and Maurice P. A. (1998) The influence of natural mineral coatings on feldspar weathering. *Nature* **395,** 588–591.

Park N-S., Kim M-W., Langford S. C., and Dickinson J. T. (1996) Atomic layer wear of single-crystal calcite in aqueous solution using scanning force microscopy. *J. Appl. Phys.* **80,** 2680–2686.

Sangwal K. (1987) Etching of crystals: theory, treatment, and application. Elsevier, Amsterdam.

Schaarwächter W. (1965a) Zum Mechanismus der Versetzungsätzung I. Die Bildung zweidimensionaler Lochkeime an den Enden von Versetzungslinien. *Phys. Status Solidi.* **12,** 375–382.

Schaarwächter W. (1965b) Zum Mechanismus der Versetzungsätzung II. Entstehungsbedingungen für Ätzgruben. *Phys. Status Solidi.* **12,** 865–876.

Schott J., Brantley S., Crerar D., Guy C., Borcsik M., and William C. (1989) Dissolution kinetics of strained calcite. *Geochim. Cosmochim. Acta* **53,** 373–382.

Stipp S. L., Eggleston C. M., and Nielsen B. S. (1994) Calcite surface structure observed at microtopographic and molecular scales with atomic force microscopy (AFM). *Geochim. Cosmochim. Acta* **58,** 3023–3033.

Teng H. H. and Dove P. M. (1997) Surface site-specific interactions of aspartate with calcite during dissolution: Implications for biomineralization. *Am. Mineral.* **82,** 878–887 No.9–10.

Teng H. H., Dove P. M., Orme C. A., and De Yoreo J. J.. (1998) The thermodynamics of calcite growth: A baseline for understanding biomineral formation. *Science* **282,** 724–727.

Teng H. H., Dove P. M., and De Yoreo J. J. (2000) Kinetics of calcite growth: Analysis of surface processes and relationships to macroscopic rate laws. *Geochim. Cosmochim. Acta* **64,** 2255–2266.

Tilley R. J. D. (1987) Defect crystal chemistry and its applications. Chapman and Hall, New York, p. 8.

Van der Hoek B., Van der Eerden J. P., and Bennema P. (1982) Thermodynamic stability conditions for the occurrence of hollow cores caused by stress of line and planar defects. *J. Cryst. Growth.* **56,** 621–632.